Journal of Luminescence 182 (2017) 107–113

Contents lists available at ScienceDirect

Journal of Luminescence

journal homepage: www.elsevier.com/locate/jlumin

Full Length Article

Study on grow process and optical properties of ZnO microrods synthesized by hydrothermal method

H. Félix-Quintero [a,b,c], J. Angulo-Rocha [b], S.H. Murrieta [c], A.J. Hernández [c], G.E. Camarillo [c], J.M.C. Flores [c], C. Alejo-Armenta [d], M. García-Hipolito [e], F. Ramos-Brito [b,*]

[a] Posgrado en Ciencia e Ingeniería de Materiales, Universidad Nacional Autónoma de México, AP 70-360, Coyoacán 04510, DF, Mexico
[b] Laboratorio de Síntesis de Materiales, Facultad de Ciencias Físico-Matemáticas, Universidad Autónoma de Sinaloa, Ciudad Universitaria S/N, CP. 80000, Culiacán de Rosales, Sinaloa, Mexico
[c] Instituto de Física, Universidad Nacional Autónoma de México, AP 20-364, Álvaro Obregón, 01000 DF, Mexico
[d] Centro de Ciencias de Sinaloa, Ave. De las Américas 2771 Nte. CP 80000, Culiacán de Rosales, Sinaloa, Mexico
[e] Instituto de Investigaciones en Materiales, Universidad Nacional Autónoma de México, AP 70-360, Coyoacán 04510, DF, Mexico

ARTICLE INFO

Article history:
Received 22 December 2015
Received in revised form
4 September 2016
Accepted 21 September 2016
Available online 19 October 2016

Keywords:
ZnO rods
Role of HMT
Strong exciton emission
Structural deffects

ABSTRACT

ZnO rods were synthesized by hydrothermal method. Physical dimensions of the ZnO rods were changed systematically as a function of: precursor salt, deposition time, molarity, and temperature parameters. Nano and Microrods were obtained by using nitrate and acetate, respectively. The morphology was obtained by Scanning Electron Microscope. Zinc acetate resulted as the optimum precursor salt to study the synthesis process of the rods. Diffuse reflectance, photo and cathode luminescence, and x-ray diffraction techniques were employed to characterize the rods as a function of hexamine molarity/zinc acetate molarity ratio (M_{HMT}/M_{Zn}). Optical results made possible to propose an energy diagram that presents different optical radiative desexcitation mechanisms. All rods resulted with an average energy gap of 3.36 eV and several energy levels into it associated to structural defects. The increase of neutral interstitial zinc and/or neutral oxygen vacancy shallow donors with the incorporation of HMT into precursor solution contributed to have a red shift of the ultraviolet emission.

1. Introduction

Transparent conducting oxide materials like zinc oxide (ZnO) and cadmium oxide (CdO) have received a vast amount of attention in the last few years. These materials are transparent and conductive with a wide variety of applications in industry and research [1]. Particularly, ZnO has drawn attention because its large energy gap (3.36 eV at room temperature) and an exciton bond energy of 60 meV making it in a candidate material for ultraviolet and blue laser devices that works at room temperature (T_{room}) [2–4]. For these reasons, the ZnO nano/micro-structures are attractive for high efficient short wavelength optoelectronics devices [3]. Plus, ZnO material is bio-safe and biocompatible so that it can be used also for medical applications without any coating [5]. Until now, have been successfully synthesized nano and micro-materials of ZnO with different morphologies and interesting structures, such as: nanowires [6,7], nanobelts [7], nanorings [8], nanobows [8], nano/microtubes [3,9], nano/microrods [2], flower-shaped [10], nanosaws [11], etc. These materials have been grown by different methods like metal organic chemical vapor deposition (MOCVD) [4], dc magnetron sputtering [1], chemical spray [12], optical thermal evaporation [9], hydrothermal solution synthesis [13], etc.

Almost all reported nano and micro-structures of ZnO exhibit visible (VIS) luminescence along with an ultraviolet (UV) luminescence [14]. The visible luminescence has been related to free carriers accumulation and defects in its crystalline structure [14,15]. The technological utility of nano and micro-materials do not depends only on the crystal quality and superficial chemistry, but also on their arrangement and special orientation [10]. Recently, the ZnO thin films with nano or micro-rod arrangement have attracted interest because they are expected to improve the performance of ZnO based devices [13]. A hydrothermal process using equimolar solutions of zinc nitrate and Hexamethylenetetramine or Hexamine (HMT) was developed by Vayssieres and coworkers to grow ZnO particles. This process not requires any membrane, template, surfactant, or an applied external field to create anisotropic particles and to control their orientation [16,17]. O′Brien and coworkers report the ZnO nanorod synthesis by

* Corresponding author.
E-mail addresses: framosbrito@uas.edu.mx, ramosbritof@gmail.com (F. Ramos-Brito).

http://dx.doi.org/10.1016/j.jlumin.2016.09.049
0022-2313/

thermal decomposition of zinc acetate in an organic solvent with the presence of oleic acid [18]. Commonly the ZnO nano/microrods result with hexagonal symmetry of Wurtzite type strongly oriented along (002) direction [18–21].

This work reports the analysis on physical dimensions and morphology differences of ZnO rods obtained by hydrothermal process. Zinc nitrate and zinc acetate were employed as precursors. The morphology and physical dimensions were analyzed as a function of synthesis temperature, synthesis time and molarity. By using Scanning Electron Microscopy (SEM) were selected those who show uniform rods regarding to morphology and physical dimensions. Once this was done, the synthesis of ZnO rods as a function of the concentration of HMT was done. This is in order to study the role of the HMT in the crystalline defect formation during synthesis process. X-ray diffraction studies (XRD), photoluminescence (PL) and cathodoluminescence (CL) studies as a function of HMT concentration were done.

2. Materials and methods

2.1. Material synthesis

ZnO rods-like were synthesized by employing Vayssieres method [16,17]. A flask containing pieces of Corning glass substrate, and an equimolar (0.05 M) aqueous solution (MilliQ 18.2 MΩ) of zinc nitrate, $Zn(NO_3)_2$ $4H_2O$, and hexamine, $(CH_2)6N_4$, were placed in a regular laboratory hot plate and heated at 85 °C for 1–5 h, depending on the required ZnO rod quantity. After analysis of ZnO rods obtained from zinc nitrate precursor it was proceeded to change it to zinc acetate dihidratate, $Zn(O_2CCH_3)$ 2middot;;$(H_2O)2$. Once zinc nitrate was replaced by zinc acetate in precursor solution, ZnO rods were synthesized considering variations in different synthesis parameters, this in order to study the synthesis process of ZnO rods as a function of those parameters. Systematic variations on both zinc acetate and hexamine molarities (M_{Zn} and M_{HMT}) and synthesis temperature (T_S) were considered. The M_{Zn} values were: 0.05, 0.025 and 0.01 mol. The M_{HMT}/M_{Zn} ratio had values of: 0, 0.6, 1.0, and 3.0. T_S was varied in a range of (85–98) °C. All samples were synthesized during 5 h.

2.2. Characterization

Micrographs to explore the morphology of the samples, and their chemical composition by EDS were obtained, both with a Leica Cambridge Stereoscan 440 Scanning Electron Microscope (SEM) equipped with a beryllium window x-ray detector. Crystalline structure was analyzed by XRD, using a Broker-axs D8-advance with Cu Kα radiation at 1.5426 Å. Identification of hexagonal phase and indexing of the peaks for the XRD patterns were carried out by using XRD-PDF cards provided by ICCD with associated numbers: 00-036-1451 for zinc oxide and 00-004-0831 for zinc. The grain size (t) was calculated by using Scherrer formula [22].

Diffuse reflectance (DR) measurements in a range of (350–1000) nm were carried out by employing a VARIAN Cary 5000 UV–vis-NIR Spectrophotometer and considering the polytetrafluoroethylene as reference material for DR=1. CL spectra were achieved in a stainless steel vacuum chamber with a cold cathode electron gun (Luminoscope, model ELM-2; MCA, Relion Co.) Samples were placed inside the vacuum and evacuated to 10^{-3} Torr. The electron gun was deflected at 90° to bombard the luminescent material perpendicular to the surface. The accelerating voltage and

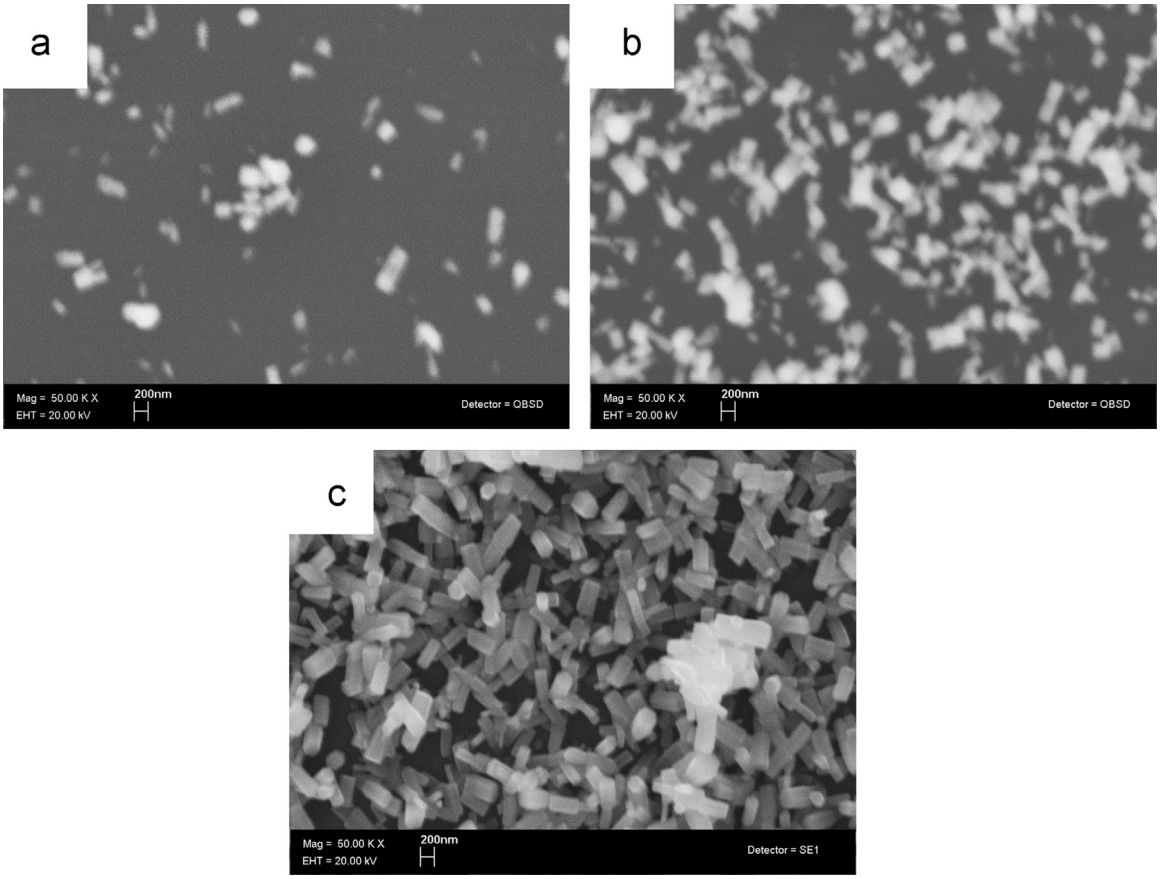

Fig. 1. Micrographs of ZnO microrods synthesized from zinc nitrate based precursor solution varying the deposition time: (a) 3 h, (b) 4 h and (c) 5 h. The other synthesis parameter values were: $M_{HMT}/M_{Zn}=1$, $M_{Zn}=0.05$ mol and $T_S=85$ °C.

the applied current were varied in a range of (1 – 15) kV and (100 – 600) μA. The spot size of the electron beam on the sample surface was approximately 5 mm in diameter, which implies current densities in a range of (0.5 – 3.1) mA/cm^2. The emitted light from the sample was collected by an optical fiber and fed into the spectrofluorimeter FluoroMax-P brand, Jobin Yvon Horiba to be analyzed. The spectrofluorimeter has a resolution <2 nm, and the lamp intensity correction is performed automatically by this instrument, which measures the excitation light intensity with an additional photomultiplier tube and performs the correction accordingly before displaying the data. All CL spectra were obtained at T_{room}.

3. Results and discussion

3.1. Morphology

Fig. 1a–c show SEM images of ZnO rods synthesized from zinc nitrate based precursor solution for three different deposition times: 3, 4 and 5 h, respectively. While Fig. 2a shows SEM image of ZnO rods synthesized from zinc acetate based precursor solution for deposition time (t_S)=4 h. ZnO rods were synthesized with the same conditions for both precursor solutions: $M_{HMT}/M_{Zn}=1$, $M_{Zn}=0.05$ mol, and $T_S=85$ °C. From Fig. 1 is notable that employing zinc nitrate, ZnO bars with dimensions of about 200 nm diameter and 400 nm length were obtained (Fig. 1c), whereas employing zinc acetate ZnO bars with dimensions of about 2 μm diameter and 10 μm length were obtained (Fig. 2a), which means a difference on dimensions in at least one order of magnitude. It can be seen from Fig. 1a–c that synthesis and grow rate in the first 3 h was lower than two hours later. This possibly means that at the beginning of the reaction, the nucleation process predominates over the grow process, maybe because nucleation requires less energy. Once the nucleation process reaches a maximum, when concentration of nuclei is high enough, the growth of rods begins but does it at high rates, predominating over the nucleation process. Once ZnO rods are close to reach submicron dimensions, probably have enough surface defects which lead again to a nucleation process that predominates over the synthesis of rods. Unlike of the synthesis process of ZnO rods by employing zinc nitrate, ZnO rods by employing zinc acetate reach higher dimensions for the same values of t_S showing a uniform growth as a function of time. This suggests that zinc acetate promotes the synthesis of ZnO rods at apparently constant rate which could enable the study of the synthesis process of the rods.

It is observable in Fig. 2a that ZnO rods form clusters at $M_{Zn}=0.05$ mol; consequently M_{Zn} was reduced, in order to reduce the ZnO rods synthesis rate. Fig. 2 shows ZnO rods for three different M_{Zn} values: 0.05 mol (Fig. 2a), 0.025 mol (Fig. 2b), and 0.01 mol (Fig. 2c), preserving $M_{HMT}/M_{Zn}=1$. For $M_{Zn}=0.025$ mol, rods with three different kinds of dimensions were synthesized (labeled in the figure), even more, tetrapods were observed too. While in Fig. 2c is clear that $M_{Zn}=0.01$ mol gives uniform synthesis as regards in physical dimensions and longer ZnO rods. Rods with diameter of 1 μm and lengths in a range of (5–20) μm were obtained, similar to rods number 2 in Fig. 2b. In order to have uniform synthesis as regards in physical dimensions, M_{Zn} was fixed at 0.01 mol value for further ZnO depositions.

From this now on, all results are referred to ZnO rods synthesized by employing zinc acetate, $M_{Zn}=0.01$ mol and $t_S=5$ h, unless otherwise stated. Figs. 3 and 2c illustrate the differences that show ZnO rods synthesized at two different temperatures, $T_S=98$ °C and

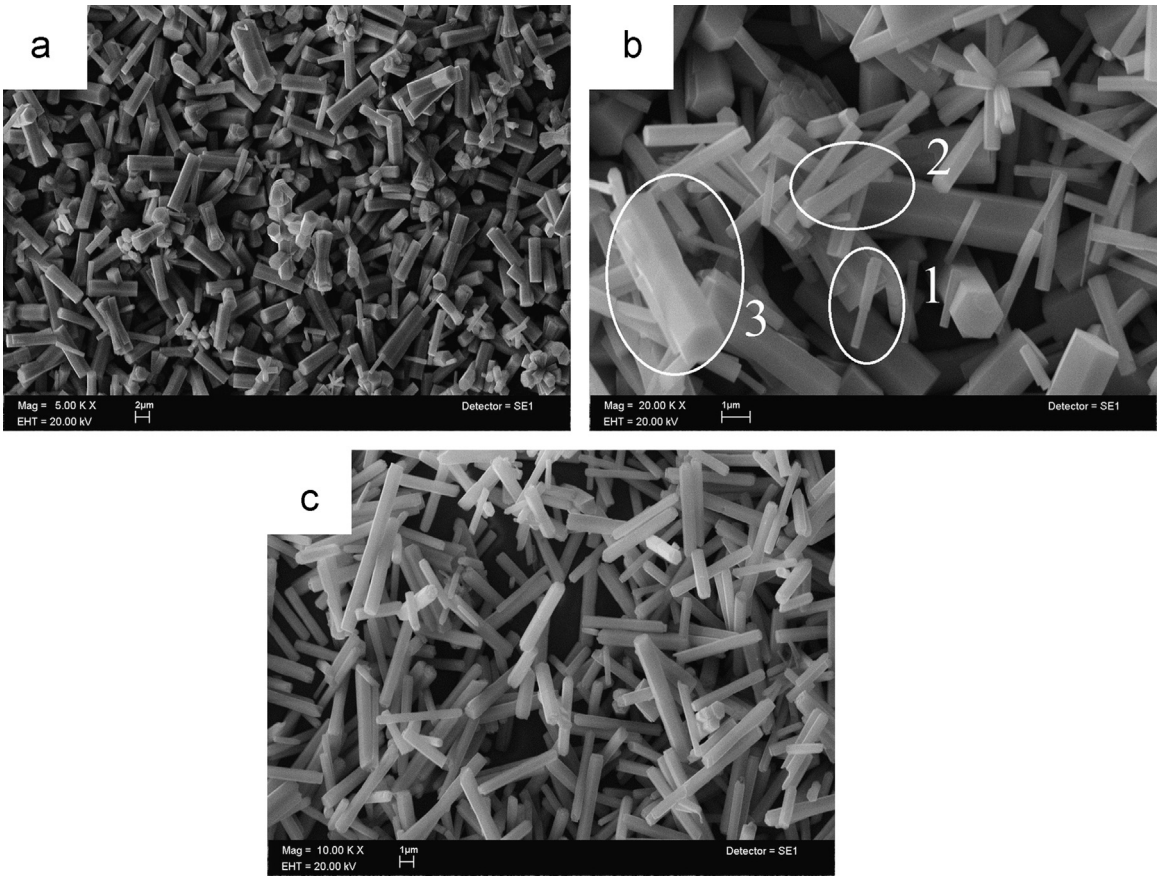

Fig. 2. Micrographs of ZnO microrods synthesized from zinc acetate based precursor solutions varying M_{Zn}: a) 0.05 mol, b) 0.025 mol and c) 0.01 mol. The other synthesis parameter values were: $M_{HMT}/M_{Zn}=1$, $t_s=4$ h and $T_S=85$ °C.

85 °C, respectively, but same values for $M_{HMT}/M_{Zn}=1$. There is one notable difference between these samples, the sample obtained at 98 °C shows nanorods and microrods simultaneously with average diameters of: 100 nm and 2 μm, respectively, and conforming an heterogeneous film; while sample obtained at 85 °C only presents microrods conforming an homogeneous film. Synthesis at 98 °C gives origin to clusters of submicron-rods as it's shown in inset of Fig. 3. In order to have homogeneous ZnO films, T_S was fixed at 85 °C for further ZnO depositions.

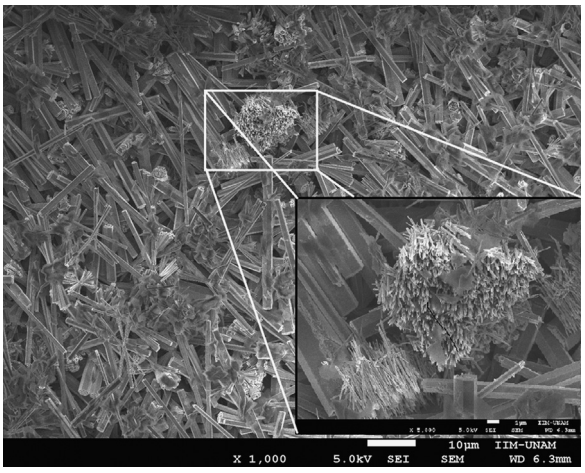

Fig. 3. Micrograph of ZnO microrods that were synthesized from zinc acetate based precursor solution and employing the synthesis parameter values: $M_{Zn}=0.01$ mol, $M_{HMT}/M_{Zn}=1$, ts = 4 h and $T_S=98$ °C. The inset shows the existence of nanobars.

The synthesis of ZnO rods by varying M_{HMT}/M_{Zn} ratio was realized in order to study its role on the morphology of the ZnO rods. Fig. 4 shows the ZnO rods synthesized by employing M_{HMT}/M_{Zn} values of: 0, 0.6, 1.0 and 3.0. It can be seen that the quantity and dimensions of ZnO rods were varied when M_{HMT}/M_{Zn} value increases. The morphological quality of the rods is increased when M_{HMT}/M_{Zn} increases. Only sample synthesized from precursor solution without HMT shows poor sintering rate with rods that have a diameter of 2 μm and lengths of 9 μm (Fig. 4a). For $M_{HMT}/$

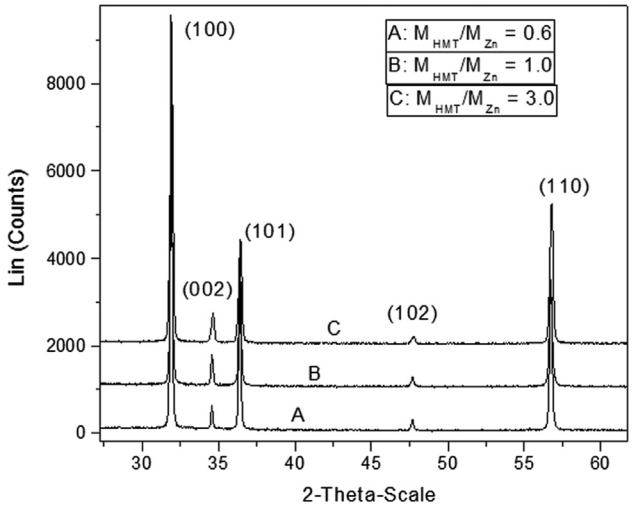

Fig. 5. X-ray diffraction pattern of ZnO rods synthesized from zinc acetate based precursor solutions as a function of M_{HMT}/M_{Zn} ratio. $M_{HMT}/M_{Zn}=0.6$ (a), 1 (b) and 3 (c).

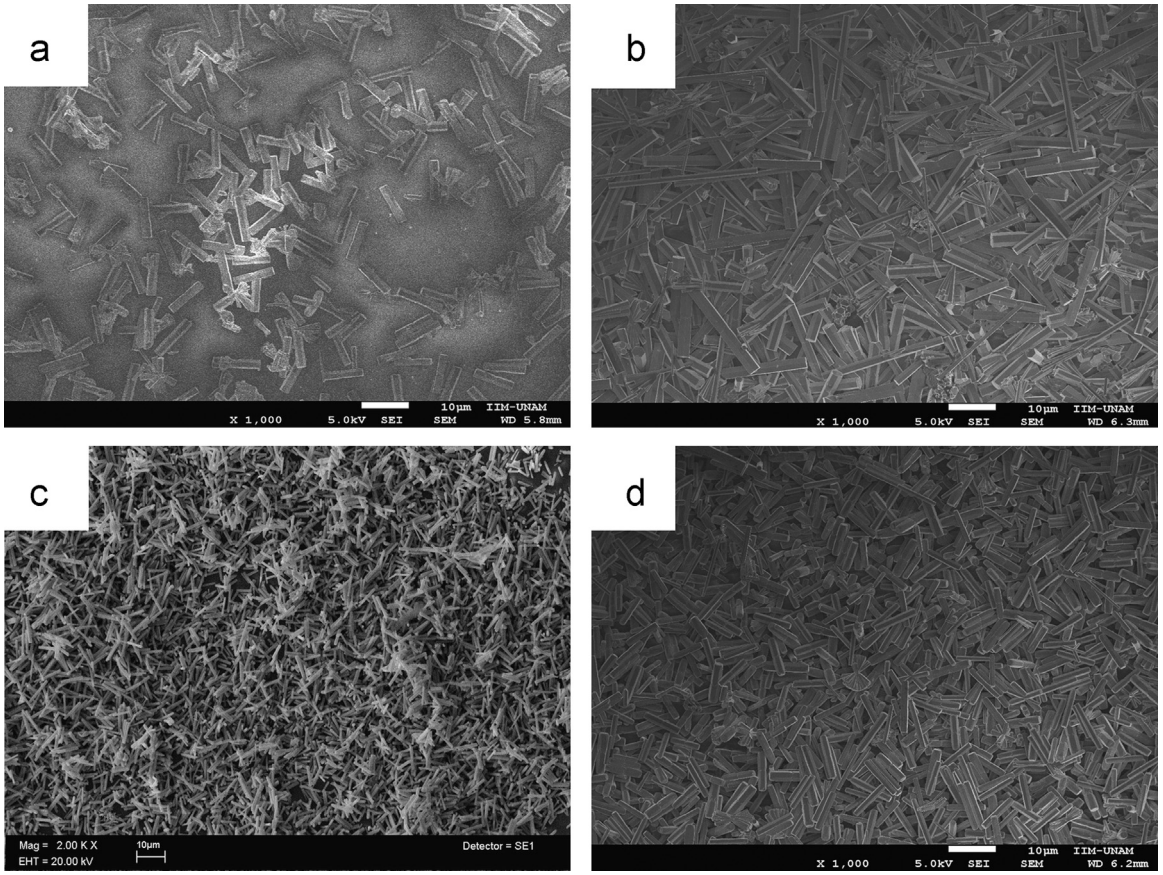

Fig. 4. Micrographs of ZnO microrods synthesized from zinc acetate based precursor solutions varying M_{HMT}/M_{Zn} ratio. $M_{HMT}/M_{Zn}=0$ (a), 0.6 (b), 1.0 (c) and 3.0 (d). The other synthesis parameter values were: $M_{Zn}=0.01$ mol, $t_s=4$ h and $T_S=85$ °C.

M_{Zn}=0.6 (Fig. 4b) there are two things to mention: variation on quantity is notable and low control of dimensions were observed, the figure shows all surface covered by rods with diameter of 1 to 3 μm and lengths of 15 to 30 μm. For $M_{HMT}/M_{Zn} \geq 1$ homogeneous films were obtained and the sintering rate of rods remains high and, apparently, its physical quality is significantly better as shown in Fig. 4c and d. The rods resulted with diameter of 1 μm and lengths of 7 μm for M_{HMT}/M_{Zn}=1 and diameter of 1.5 μm and lengths of 8.5 μm for M_{HMT}/M_{Zn}=3. The length/diameter ratio (l/d) values of the rods as a function of M_{HMT}/M_{Zn} were: 4.5, 15–30, 7, and 5.6 for: 0, 0.6, 1 and 3, respectively.

It is well known that ZnO crystal exhibits partial polar characteristics, and in a typical Wurtzite structure the (001) plane is the basal polar plane. One end of the basal polar plane terminates with partially positive Zn lattice points and the other end terminates in partially negative oxygen lattice points [23]. In chemical synthesis processes, hexamine being a non-polar chelating agent would preferentially attach to the non-polar facets of the rods, thereby exposing only the (002) plane for growth. Thus a preferential growth along (0002) direction is made possible.

The M_{HMT}/M_{Zn} ratio plays an important role in ZnO rods synthesis process, varying its value is possible to modify its physical dimensions, increase its morphological quality and influence on its l/d ratio. An intensive study in this direction is necessary in order to understand better the influence of HMT in synthesis process.

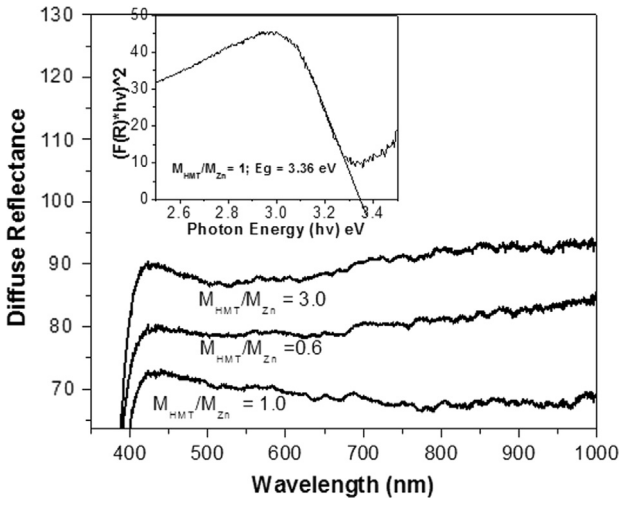

Fig. 6. Diffuse Reflectance spectra of ZnO rods synthesized as a function of M_{HMT}/M_{Zn} ratio. Inset in figure shows the energy gap.

3.2. Crystalline structure

The X-Ray diffraction analysis in Fig. 5 shows dominance of the (100), (101), (110), (002) and (102) crystallographic planes corresponding to a ZnO Wurtzite lattice and no others planes were observed, all patterns corresponds to ZnO Wurtzite hexagonal structure, with lattice parameters: a=3.24982 and c=5.2061 in accordance to XRD-PDF card number 00-036-1451. The centers of the XRD peaks were not shifted when M_{HMT}/M_{Zn} varies indicating not lattice distortion. The average grain size obtained was 50 nm.

From the morphology study, the films were conformed by ZnO rods that are lying down indicating a preferential growth on (002) planes, in agreement with the relative intensity of the XRD peaks that show a preferential growth of (100) planes.

3.3. Chemical composition

The chemical composition of the ZnO rods as a function of M_{HMT}/M_{Zn} ratio was: 52.72% O, 44.34% Zn, 2.16% Si, and 0.78% Ca; 53.02% O, 46.26% Zn, and 0.72% Si; 54.16% O and 45.84% Zn; 52.98% O and 47.02% Zn; for M_{HMT}/M_{Zn}=0, 0.6, 1.0 and 3.0, respectively. The presence of Si, Ca and excess oxygen in M_{HMT}/M_{Zn}=0 and M_{HMT}/M_{Zn}=0.6 samples was associated to the glass substrate, in these samples the electron beam penetrates up to the glass substrate, the absence of Si and Ca in the samples with M_{HMT}/M_{Zn}=1.0 and 3.0 indicates that the Zn and O contents were associated to ZnO rods only, that shows a relative oxygen excess. It was reported that the role of hexamine in the growth of ZnO structures in the hydrothermal process is mainly as a pH buffer by a slow release OH^- ions, through thermal decomposition [24], the oxygen excess in ZnO rods can be due to zinc vacancies, interstitial oxygen, oxygen anti-site and/or the presence of OH^- ions.

3.4. Optical properties

Fig. 6 shows the DR spectra for the M_{HTT}/M_{Zn}=0.6, 1.0 and 3.0 samples in spectral region 350–1000 nm. The inset shows the plot of $(F(R)^*h\nu)^2$ vs hν that gives average gap value of: 3.36 eV. It was not possible to obtain the diffuse reflectance spectrum for the M_{HMT}/M_{Zn}=0.0 sample because it has a very poor ZnO synthesis.

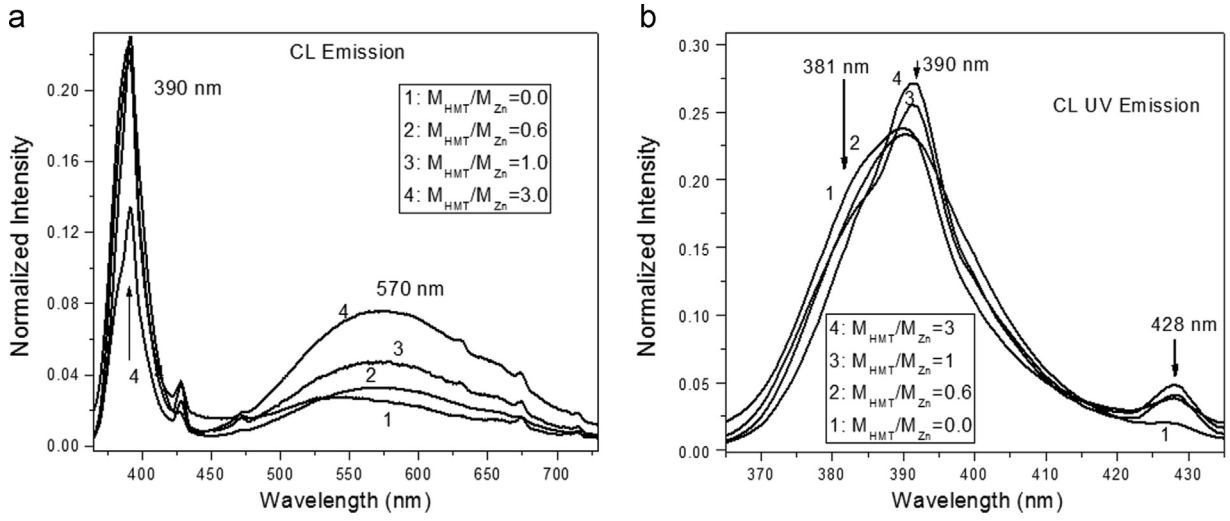

Fig. 7. Normalized cathodoluminescence emission of ZnO rods as a function of M_{HMT}/M_{Zn} ratio. M_{HMT}/M_{Zn}=0 (1), 0.6 (2), 1.0 (3) and 3.0 (4). Figure b shows the normalization of the UV region.

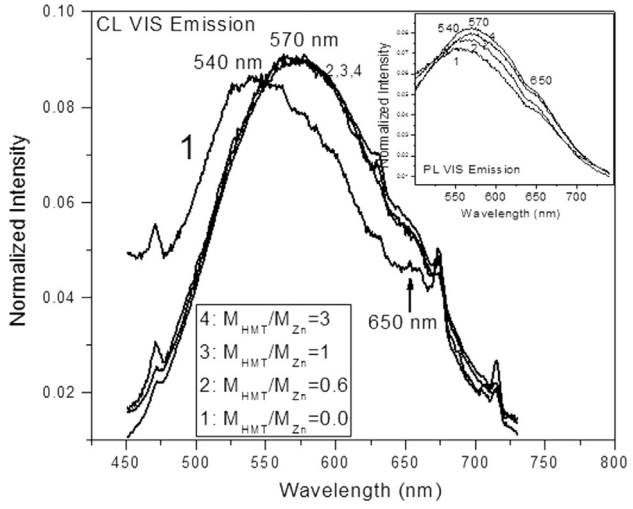

Fig. 8. Normalized cathodo and photoluminescence (inset) emissions of ZnO rods as a function of M_{HMT}/M_{Zn} ratio in VIS region. $M_{HMT}/M_{Zn}=0$ (1), 0.6 (2), 1.0 (3) and 3.0 (4).

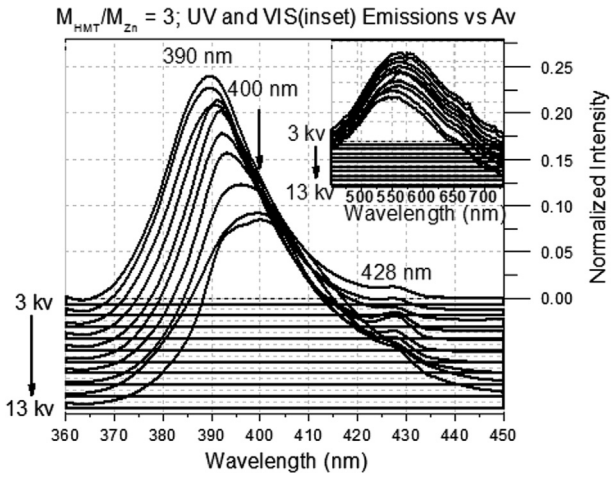

Fig. 9. Normalized cathodoluminescence emission spectrum of ZnO rods as a function of acceleration voltage with VIS region in inset.

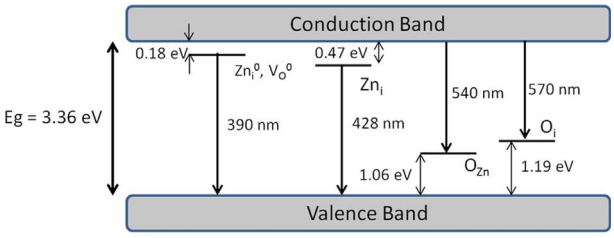

Fig. 10. Energy diagram showing the electronic transitions and structural defects that were responsible of the CL and PL emission of ZnO rods.

The DR spectra show a wide absorption along all visible spectra that looks conformed by two wide bands centered at 550 and 800 nm. The absorption is associated with electronic transitions from valence band (VB) to energy levels incorporated into band gap due to the presence of structural defects.

Fig. 7 shows the normalized CL emission of ZnO rods as a function of M_{HMT}/M_{Zn} ratio. All spectra show two structured wide emission bands centered at: UV and VIS regions. After comparison of CL spectra, all of them result practically the same with exception of CL spectrum for sample that results from precursor solution without HMT ($M_{HMT}/M_{Zn}=0.0$) where red shifts of the maxima of the UV and VIS emission bands become obvious.

Fig. 7b shows a structured emission band in the UV region with peaks centered at: 381 nm (3.25 eV), 390 nm (3.18 eV), and 428 nm (2.89 eV), associated to electronic transitions. The first band is associated with electronic transition from conduction band (CB) to valence band and exciton emissions [25,26], a low temperature study is necessary to resolve this band. The 390 nm band suggest the existence of shallow donors sites at 0.18 eV below the CB, commonly associated to neutral interstitial zinc (Zn_i^0) and oxygen vacancies (V_O^0), consequently to electronic transitions: $Zn_i^0 \rightarrow VB$ and $V_O^0 \rightarrow VB$ [27,28]. Violet emission (428 nm) that was reported already by different authors [27,29,30], has been associated to the presence of interstitial zinc (Zn_i) at 0.47 eV below conduction band giving the $Zn_i \rightarrow VB$ electronic transition. The change of the relative intensities of 381 and 390 nm bands of UV emission, obtained when M_{HMT}/M_{Zn} increased, was associated to the increment on intensity of the 390 nm emission band that corresponds to an increment on content of Zn_i^0 or V_O^0. The increment of violet emission means an increment of Zn_i defect when HMT is added.

In Fig. 8 is shown the CL and PL (inset) spectra in visible region, which resulted similar between them. Both emissions were composed by bands centered at: 540 nm (2.30 eV), 570 nm (2.17 eV), and 650 nm (1.90 eV). The green emission (540 nm) is related to oxygen anti-site (O_{Zn}) [28,30,31] and V_O [29,32,33] that could be a transition from CB to O_{Zn} or from shallow donor V_O^0 to O_{Zn} or from CB to V_O. In this case the green emission was associated to CB→O_{Zn} transition because in synthesis processes under oxygen rich conditions, O_{Zn} defect has the one of the lowest formation energy [34]. The emission centered at 570 nm is commonly associated to interstitial oxygen (O_i) [31,35], however, Djurišić et al. shows evidence that this emission is due to the presence of hydroxyl groups [36]. The red shift of the visible emission band when HMT is added could indicate an increment of O_i defects or the presence of hydroxyl groups, future studies should be done to elucidate this. For the orange-red region (650 nm) recent studies have demonstrated that this emission is related to zinc vacancies (V_{Zn}) or excess oxygen [36,37], but is still controversial. In this case this emission was associated to V_{Zn} defect supported on: a) O_{Zn} emission dominates the visible region, namely for the sample synthesized without HMT, and for samples with $M_{HMT}/M_{Zn} \geq 0.6$ the dominant emission is due to OH^- groups and b) the orange-red emission seemingly remains constant with and without HMT. The invariability of visible emission CL or PL spectra for $M_{HMT}/M_{Zn}=0.6$, 1.0 and 3.0 indicates that the relative concentration of structural defects remains constant as a function of M_{HMT}/M_{Zn} ratio.

In order to study the films optical quality the UV emission intensity / VIS emission intensity (I_{UV}/I_{VIS}) ratio as a function of M_{HMT}/M_{Zn} was calculated. The values of I_{UV}/I_{VIS} were: 2.22, 1.45, 0.96 and 0.28 for $M_{HMT}/M_{Zn}=0$, 0.6, 1 and 3, respectively. These values indicate that the incorporation of HMT into precursor solution means an increase in the content of defects, which means a lost in optical quality that is accentuated when HMT content increases. A systematic study that considers more M_{HMT}/M_{Zn} values in the 0–3 range must be done in order to find a correlation between I_{UV}/I_{VIS} and M_{HMT}/M_{Zn} variables.

Fig. 9 shows the CL emission spectra as a function of acceleration voltage (Av) for sample with lower I_{UV}/I_{VIS} value ($M_{HMT}/M_{Zn}=3$). The UV emission shows that the exciton emission is lost and defect related emission centered around 400 nm increases, as Av is increased. This was associated to the increment of thermal energy of the sample when Av increases. The analysis of VIS emission (inset) shows that there was not preference over the excitation of a kind of defect when Av increases which means that the relative concentration of defects remains constant as a function of depth.

Fig. 10 presents the energy diagram that shows the electronic transitions and structural defects that were responsible of the CL and PL ZnO rods emission.

4. Conclusions

Hydrothermal method was employed to synthesize ZnO rods with Wurtzite hexagonal crystalline structure with micro and submicron dimensions. Physical dimensions of the ZnO rods were changed systematically as a function of: precursor salt, Ts, M_{Zn} and M_{HMT}/M_{Zn} parameters. The intrinsic rod shape morphology and crystalline structure remains for different parameter values. Zinc acetate resulted the optimum precursor salt to study the synthesis process of the rods because promotes the synthesis of ZnO rods at apparently constant rate. The optimum parameters values were: Ts = 85 °C, M_{Zn} = 0.01 mol and $M_{HMT}/M_{Zn} \geq 1$ that give homogeneous films conformed by ZnO rods that present uniform synthesis as regards in physical dimensions, long rods and high sintering rate. The M_{HMT}/M_{Zn} ratio plays an important role in ZnO rods synthesis process, varying its value is possible to modify its physical dimensions, increase his morphological quality and influence on its length/diameter ratio.

Optical results made possible to propose an energy diagram that presents different optical desexcitation mechanisms in the region UV–vis. All ZnO rods resulted with an average energy gap of 3.36 eV and several energy levels into it associated to structural defects. The structural defects that were responsible of VIS emission are: zinc vacancies, interstitial zinc, oxygen vacancies, interstitial oxygen and oxygen anti-site and their relative concentration remains constant as a function of M_{HMT}/M_{Zn} and material depth. However, although there were not variations in the relative contents of defects when HMT content in precursor solution varies, an increment of the total content of defects with the increase of M_{HMT}/M_{Zn} ratio resulted.

The use of HMT produces a red shift of both UV and VIS emissions, that were associated to the increment of Zn_i, Zn_i^0 and V_O^0 point defects, and the excess of oxygen (O_i and/or OH^-), respectively.

Acknowledgments

Omar Novelo, Adriana Tejeda and Zacarías Rivera for technical support provided, Secretaria de Educación Pública (SEP) (Grant number DSA/1035/14/10808) under its PROMEP program, and Universidad Autónoma de Sinaloa (UAS) (Grant number PROF2014) under its PROFAPI program, SEP (México) and UAS (Sinaloa-México) for the financial grant for this investigation.

References

[1] A.K. Chawla, D. Kaur, R. Chandra, Opt. Mater. 29 (2007) 995.
[2] Y. Gu, Igor L. Kuskovsky, M. Yin, S. O´Brien, G.F. Neumark, Appl. Phys. Lett. 85 (17) (2004).
[3] Meng-Ke Li, De-Zhen Wang, Sheng Ding, Yong-Wen Ding, Jun Liu, Zhao-Bin Liu, Appl. Surf. Sci. 253 (2007) 4161.
[4] W.J. Shen, J. Wang, Q.Y. Wang, Y. Duan, Y.P. Zeng, J. Phys. D: Appl. Phys. 39 (2006) 269.
[5] Gyu-Chul Yi, Chunrui Wang, Won Il Park, Semicond. Sci. Technol. 20 (2005) 22.
[6] Chen-Hao Ku, Jih-Jen Wu, Nanotechnology 18 (2007) [505706 (9pp].
[7] Xudong Wang, Jinhui Song, Zhong Lin Wang, J. Mater. Chem. 17 (2007) 711.
[8] William L. Hughes, Zhong L. Wang, Appl. Phys. Lett. 86 (2005) 043106.
[9] Q.P. Ding, Q.Q. Cao, H.B. Huang, S.G. Yang, X.N. Zhao, Y.W. Du, J. Phys. D: Appl. Phys. 39 (2006) 46.
[10] J.W. Zhao, L.R. Qin, Z.D. Xiao, L.D. Zhang, Mater. Chem. Phys. 105 (2007) 194.
[11] S.G. Hussain, et al., J. Phys. D: Appl. Phys. 40 (2007) 7662.
[12] L. Castañeda, A. García-Valenzuela, E.P. Zironi, J. Cañetas-Ortega, M. Terrones, A. Maldonado, Thin Solid Films 503 (2006) 212.
[13] Min Guo, Peng Diao, Shengmin Cai, Thin Solid Films 515 (2007) 7162.
[14] J. Antony, X.B. Chen, J. Morrison, L. Bergman, Y. Qiang, Appl. Phys. Lett. 87 (2005) 241917.
[15] Q.X. Zhao, P. Klason, M. Willander, H.M. Zhong, W. Lu, J.H. Yang, Appl. Phys. Lett. 87 (2005) 211912.
[16] L. Vayssieres, Adv. Mater. 15 (2003) 464.
[17] L. Vayssieres, K. Keis, S.E. Lindquist, A. Hagfeldt, J. Phys. Chem. B 115 (2001) 3350.
[18] O´Brien, et al., J. Am. Chem. Soc. 126 (2004) 6206.
[19] Changsong Liu, Yoshitake Masuda, Yunying Wu, Osamu Takai, Thin Solid Films 503 (2006) 110.
[20] E.K. Suh Ahmad Umar, Yoon-Bong Hahn, J. Phys. D: Appl. Phys. 40 (2007) 3478.
[21] S. López-Romero, M. García-H, WJCMP 3 (2003) 152.
[22] B.D. Cullity, Elements of X-Ray diffraction, First Edition, Addison-Wesley Publishing Company, Massashusetts, 1956.
[23] X.Y. Kong, Z.L. Wang, Appl. Phys. Lett. 84 (2004) 975.
[24] L. Vayssieres, J.H. Guo, J. Nordgren, J. Nanosci. Nanotechnol. 1 (2001) 385.
[25] C.H. Chia, W.C. Tsai, J.W. Chiou, J. Lumin. 136 (2013) 160.
[26] J. Rodrigues, et al., Nanotechnology VII 9519 (2015) 951906.
[27] S.A.M. Lima, F.A. Sigoli, M. Jafelicci Jr., M.R. Davolos, Int. J. Inorg. Mater. 3 (2001) 749.
[28] C.X. Xu, et al., Nanotechnology 15 (2004) 856.
[29] C.H. Ahn, et al., J. Appl. Phys. 105 (2009) 013502.
[30] M. Willander, et al., Materials 3 (2010) 2643.
[31] Bixia Lin, Zhuxi Fu, Yunbo Jia, Appl. Phys. Lett. 79 (2001) 943.
[32] Y. Dai, Y. Zhang, Q.K. Li, C.W. Nan, Chem. Phys. Lett. 358 (2002) 83.
[33] V. Khranovskyy, V. Lazorenko, G. Lashkarev, R. Yakimova, J. Lumin. 132 (10) (2012) 2643.
[34] R. Vidya, et al., Phys. Rev. B 83 (2011) 045206.
[35] Sun, et al., Nanoscale Res. Lett. 6 (2011) 556.
[36] A.B. Djurisic, et al., Nanotechnology 18 (2007) 095702.
[37] A.B. Djurisic, Y.H. Leung, K.H. Tam, L. Ding, W.K. Ge, H.Y. Chen, S. Gwo, Appl. Phys. Lett. 88 (2006) 103107.